JTTEE5 14:405-413
DOI: 10.1361/105996305X59350
1059-9630/$19.00 © ASM International

Study of the Properties of WC-Co Nanostructured Coatings Sprayed by High-Velocity Oxyfuel

J.M. Guilemany, S. Dosta, J. Nin, and J.R. Miguel

(Submitted September 21, 2004; in revised form March 14, 2005)

Interest in nanomaterials has increased in recent years. This is due to the potential improvement that size reduction to nanometric scale could provide in properties like hardness, toughness, wear, and corrosion resistance. The current study is focused on WC-Co cermets, materials that are extensively used in applications requiring wear resistance. Two coatings were sprayed by high-velocity oxyfuel using both conventional and nanostructured cermets. Both materials were characterized by means of x-ray diffraction and scanning electron microscopy to study their phases and morphology. Cross-sectional images and microhardness values are given for both coatings. Friction wear resistance of the coatings was studied by ball-on-disk (ASTM G99-90), and abrasive wear resistance was quantified by rubber-wheel (ASTM G65-91). Finally, the corrosion resistance was studied by electrochemical techniques. Comparative results showed that the nanostructured coating has better properties than the conventional coating except in the dry abrasion wear test, where the wear rates are very similar.

Keywords corrosion of high-velocity oxyfuel coatings, friction and wear, nanostructured coatings, nanostructured WC/Co coatings

1. Introduction

Lately, an increasing interest in nanostructured materials has been observed, especially for WC-Co (Ref 1-3), Al_2O_3 (Ref 4, 5), Al_2O_3/TiO_2 (Ref 6, 7), and PSZ (Ref 8) systems. Because the most common application of nanostructured materials in the thermal spray industry is for WC-based cermets, the amount of work being done related to this material is increasing quickly.

The use of materials with reduced WC grain size has improved some properties like hardness and toughness, and even sliding (Ref 9) and abrasion (Ref 10) resistance, for both bulk and sintered materials. However, for thermal spray coatings, in which the spraying process and the properties of feedstock materials have a great importance, wear resistance is normally lower than that of conventional coatings. This lack of performance of thermally sprayed nanostructured coatings has been attributed to their higher tendency to decarburization, as the surface-to-volume ratio of the WC-nanosized grains is higher than that of their conventional counterparts (Ref 1).

Considerable effort has been devoted to studying the effect of the Co binder phase percentage on the properties of the coatings (Ref 2), and mainly on the effect of spraying conditions (Ref 1, 11). In those studies, adhesion between splats and the level of decarburization were found to have an important role in the microstructure and properties. Decarburization has an effect not only on hardness but also on wear properties, as reported by Qiao et al. (Ref 1), and, thus, spraying parameter optimization is crucial.

It is well known that WC-Co coatings have a limited corrosion resistance in comparison with WC-CoCr or WC-Ni because of the electrochemical properties of the cobalt itself (Ref 12). However, using the same material, corrosion resistance can be enhanced by reducing the porosity, avoiding cracks, and increasing intersplat adhesion. For those reasons, if the use of nanostructured feedstocks can produce these improvements in microstructure and bonding, then nanostructured coatings can be expected to have better behavior on aggressive media. Unfortunately, the use of some porous shell-like nanostructured feedstock particles can induce higher levels of porosity due to heterogeneous melting (Ref 13), and unsuitable spraying conditions can lead to excessive decarburization, causing weak intersplat boundaries (Ref 1). For those reasons, some authors (Ref 1, 11, 13) have made claims for process optimization (including feedstock powders), whereas others have reported that modifying the standard parameters is detrimental for some properties (Ref 2).

The objective of this work was to study the properties of nanostructured as well as conventional WC-12Co coatings that were obtained under conventional powder-spraying conditions. The reason for that is to establish the need for further optimization of the spraying conditions for nanostructured powders.

2. Experimental Procedure

The materials used were commercially available conventional and nanostructured WC-Co powders that were produced by an agglomeration method, with mean particle sizes of 35 and 23 μm, respectively, for conventional and nanostructured powders. More details on the composition and particle size (according to the manufacturer) (H.C. Starck, Leverkusen, Germany;

J.M. Guilemany, S. Dosta, J. Nin, and **J.R. Miguel,** Thermal Spray Center, Materials Engineering, Department of Enginyeria Quimica i Metallúrgia, Universitat de Barcelona, C/Martí i Franqués, 1, E-08028 Barcelona, Spain. Contact e-mail: cpt@material.qui.ub.es.

Table 1 Feedstock powders used in this study

Coatings	Material supplier	Size distribution	Co, wt.%	WC grain size
Conventional	H.C. Starck	−45 ± 15 μm	12	1–4 μm
Nanostructured	Inframat Corp.	−45 ± 5 μm	12	50–500 nm

Inframat Corp., Farmington, CT) of these feedstock powders are presented in Table 1. To avoid different behaviors during flight in the spraying process, the selected powders had the same porous morphology. They were sprayed on two types of UNS G41350 steel coupons: flat substrates (100 × 20 × 5 mm); and cylindrical substrates (∅ = 25.4 mm, height 25.4 mm). The substrates were previously degreased with acetone and grit-blasted with white corundum at 5.6 bar, 45°, using a blasting distance of 250 mm. The grit-blasted substrates had a roughness (Ra) between 4 and 5 μm.

All the samples were sprayed using a Sulzer Metco (Westbury, NY) Diamond Jet Hybrid DJH 2700 high-velocity oxyfuel (HVOF) spraying equipment. Propylene was used as the fuel gas. Optimization of the spraying conditions was performed to decrease the decarburization of the materials in the conventional powder. The deposition parameters, recommended by Sulzer Metco for conventional WC-Co powders are presented in Table 2. These parameters are said to be the optimum for conventional powders to achieve a good combination of deposition efficiency and properties, although, as was mentioned in the introduction, some authors claim that these parameters might not be the best for the nanostructured powder (Ref 1, 11, 13).

The nomenclature of the samples is C1 for conventional coatings and N1 for nanostructured coatings. The characterization of the samples included cross-sectional scanning electron microscope (SEM) images and EDS phase analysis. The nanostructured coating was also studied by transmission electron microscopy (TEM). A more accurate phase analysis of the starting powders and coatings was performed by x-ray diffraction (XRD), including a semiquantitative analysis of the crystalline phase by the Chung method (Ref 14, 15). Cross-sectional microhardness measurements were performed by means of Vickers indentation at load of 300*g*. The indentations were measured with an optical microscope to increase measurement accuracy. Quoted values are an average of 20 indentations for each coating. Image analysis software (Matrox Inspector, version 1.71, Matrox, Dorval, Canada) was used to quantify the coating porosity. The quoted values are an average of 10 areas measured at the same magnification for each coating.

Two kinds of wear tests were performed to compare the wear resistance of both conventional and nanostructured coatings. A sliding wear test was performed using a ball on disk (BOD), ASTM G99-90 (Ref 16), in three samples of each coating deposited onto cylindrical coupons. The test diameter was 16 mm, the counterpart was a WC-Co ball, the sample relative velocity was 131 rpm, with a total testing distance of 1000 m. Humidity and temperature were kept below 20% and 25 °C, respectively. Dry abrasive tests carried out using a rubber wheel (ASTM G65-91 D) (Ref 17), with a rotating speed of 139 rpm, a load of 50 N, and a SiO_2 flux between 250 and 310 g/min. The duration of the test was 30 min, and the material loss was measured by weighting the samples every 1 min for 5 min, and then every 5 min until the end of the test. Three samples of each coating were tested. A theoretical density of 14 g/cm^3 was used to transform the mass into volume to express the wear rate in terms of material removed.

Table 2 Spray parameters used for conventional and nanostructured powders

Spray parameter	Pressure bar	Pressure psi	Flow rate L/min	Flow rate FMR
Oxygen (O_2)	10.3	150	253	40
Propylene (C_3H_6)	6.9	100	77	40

Note: FMR, flow meter reading

The corrosion resistance of the samples was evaluated by electrochemical measurements in 80 mL of an aerated and unstirred 3.4% NaCl solution. An Ag-AgCl, KCl-saturated electrode, connected to the solution through a Luggin capillary, was used as the reference electrode and a Pt-network was the auxiliary electrode. A working electrode of each coated sample was fixed at the bottom of the electrochemical cell, exposing an area of 1 cm^2 to the solution.

Open-circuit potential (E_{OC}) and electrochemical impedance (EIS) measurements were done using the EG&G Princeton Research Potentiostat/Galvanostat (Princeton, NJ) and Solartron-SI1255 systems (Solartron, Farnborough, Hampshire, UK) in a corrosion cell based on the Avesta model with few modifications. The EIS tests were carried out by applying 5 mV (rms) to the E_{OC} value, starting from 50 to 10 kHz with 7 points/decade once the E_{OC} attained the steady-state condition (after 18 h of immersion). A Pt electrode of small area, which was connected to the reference via a capacitor of 10 μF to minimize the phase shift at high frequencies (Ref 18), was used as the fourth electrode. The experimental data were fitted using the software developed by Boukamp (Ref 19).

Open-circuit potential (E_{OC} versus time) and polarization curve (C_P) measurements were done using an EG&G Parc-273. Polarization experiments were carried out in a potential range from –100 to +350 mV versus an E_{OC} at 0.166 mV/s. All electrochemical experiments were performed at room temperature. A salt fog spray test (ASTM B117-90) (Ref 20) was carried out with a 5% NaCl solution at 35 °C, 15 mm^3/h of collected solution, and 1 bar.

3. Results and Discussion

3.1. Structural Characterization

3.1.1 Powders. Figure 1 shows SEM images of conventional (Fig. 1a) and nanostructured (Fig. 1b) powders. There is an evident size difference between WC grains. Conventional WC grains have a mean size of 3 μm. According to the manufacturer, the nanostructured WC mean grain size should be between 50 and 500 nm. However, SEM images show WC grains of >500 nm. As a result, this powder should be termed *near-nanostructured* because true nanostructured materials are at scales of <100 nm. The XRD study of the initial phases of the materials showed no differences. They both were pure, containing only the desired phases: WC and Co. No traces of η-carbide phases (W_6Co_6C, W_3Co_3C) were observed.

3.1.2 Coatings. The SEM cross-sectional images of the conventional C1 (Fig. 2a) and nanostructured N1 (Fig. 2b) as-

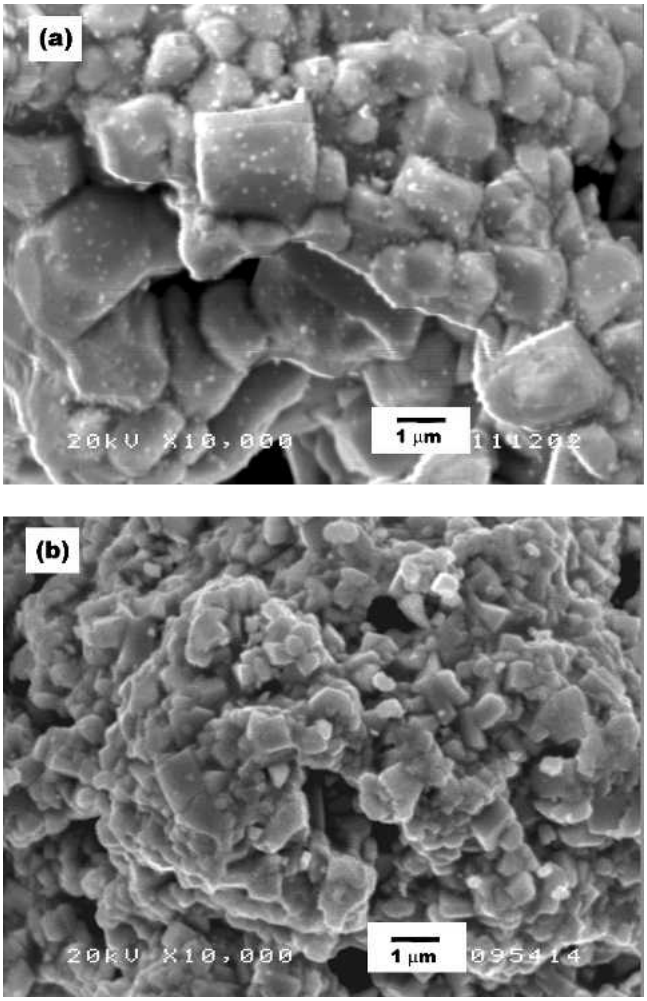

Fig. 1 SEM images of (a) conventional powder and (b) nanostructured powder

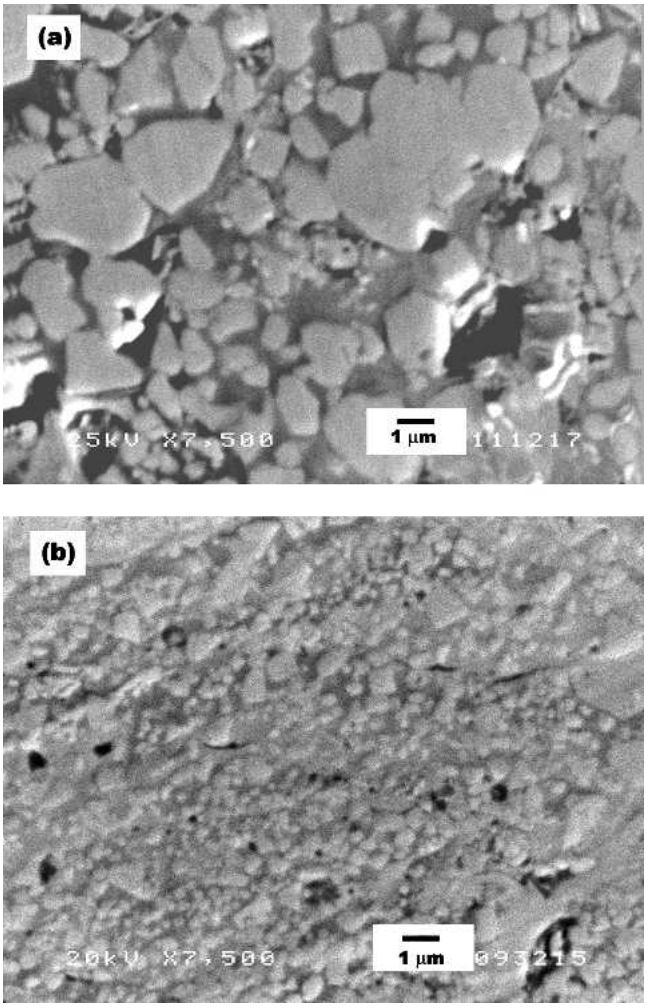

Fig. 2 SEM cross-sectional images of (a) conventional C1 coating and (b) nanostructured N1 coating

sprayed coatings are shown in Fig. 2. In the conventional structure C1, WC grains are clearly seen, whereas in the N1 coating there is a finer dispersion of smaller carbides.

There is no apparent change in carbide size for C1 after the spraying process, whereas in N1 it is difficult to quantify by image analysis. However, according to other authors, backscattered electron images show more dissolution of WC grains in the N1 coating because there are large areas where the contrast of the Co phase has been lightened due to the dissolution of WC (Ref 21, 22). The degradation reactions that take place during thermal spraying have been described (Ref 21) as:

$$2WC + O_2 \leftrightarrow W_2C + CO_2 \quad \text{(Eq 1)}$$

$$W_2C + 1/2O_2 \leftrightarrow W_2(CO) \quad \text{(Eq 2)}$$

$$W_2(CO) \leftrightarrow 2W + CO \quad \text{(Eq 3)}$$

These reactions take place mainly in WC grains that interact with oxygen. In addition, WC grains can be degraded in an oxygen-free atmosphere (i.e., those that are in the core of the particles), according to Eq 4:

$$2WC \leftrightarrow W_2C + C \quad \text{(Eq 4)}$$

According to some authors (Ref 21, 22), two types of W_2C can be formed. The first type takes place when WC grain decomposes following Eq 1 or Eq 4. The other mechanism takes place during the solidification of the Co-rich matrix leading to the precipitation of the W_2C phase in the boundaries of the WC grains. The later W_2C appears as globular fringes around the WC grains. As a consequence of these degradation reactions, some C is dissolved in the matrix. Once dissolved in the liquid, some C diffuses and reacts with the oxygen in the surface to form CO/CO_2, thus losing part of the C from the original powder. The retained C in the matrix with some W present in the liquid enriches the Co matrix to create amorphous and nanocrystalline regions. These small crystallites were found to be <8 nm (Ref 22, 23).

Depending on the degree of decarburization, metallic tungsten can precipitate near the splat boundaries (Ref 1) where there is a C depletion due to its reaction with oxygen. Also, depending

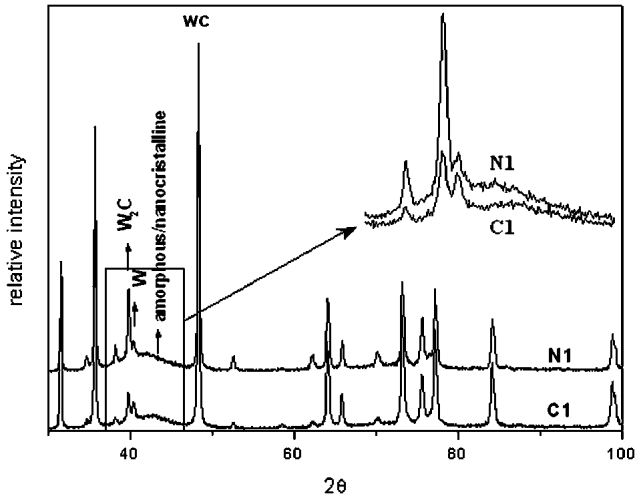

Fig. 3 XRD analysis of the nanostructured (N1) and conventional (C1) coatings.

on the degree of decarburization, the precipitation of η-phases can take place as follows (Ref 21):

$$4Co + 4WC + O_2 \leftrightarrow 2Co_2W_4C + 2CO \quad \text{(Eq 5)}$$

$$3Co + 3WC + O_2 \leftrightarrow Co_3W_3C + 2CO \quad \text{(Eq 6)}$$

$$12Co + 12WC + 5O_2 \leftrightarrow 2Co_6W_6C + 10CO \quad \text{(Eq 7)}$$

This experimental observation has been confirmed by XRD analysis, in which the nanostructured coating contains a higher fraction of W_2C.

Figure 3 shows the XRD analysis of the samples. There is an amorphous zone at 2θ angles between 35° and 48° for both coatings, although the nanostructured sample has a higher fraction of amorphous phase. Both powders suffer the typical decarburization, but the extent of this reaction is lower for the conventional powder. The nanostructured powder has a greater decarburization caused by the large surface-to-volume ratio of the WC particles. Another reason for this higher decomposition could be the agglomerated particle size. In addition to having sub-micron-sized WC grains, the nanostructured powder has a finer agglomerate size distribution than the conventional one, causing the powder to interact to a larger extent with the flame.

Trying to deeply characterize the decarburization ratio, the Chung method (Ref 14, 15) was used. The crystalline phases of each coating were quantified using the most intense peaks for each phase. This method allows the calculation of the ratio between crystalline phases by taking the relative intensity of the peaks and a k factor that depends on the ratio between the intensity of each phase and a diffraction pattern, which was a characteristic constant for each of the existing phases. Table 3 shows the semiquantitative percentages of the three main phases of the sprayed coatings.

These measurements provide evidence of the higher level of decarburization of the N1 coatings, because there is a decrease of about 15% in the sample WC content when using nanostructured powder. The W_2C-to-WC ratio increases as decarburization increases (Ref 24).

Table 3 Semiquantitative analysis of the crystalline phases by the Chung method

Coatings	WC, %	W_2C, %	W, %
Conventional C1	89	8	3
Nanostructured N1	75	22	3

Porosity measured by image analysis was 2.3% ± 0.2% for the conventional coating and 1.5% ± 0.2% for the nanostructured coating. The pores are randomly scattered throughout the cross section. Pores can be found either in the amorphous matrix or in the WC-matrix boundaries. Intersplat boundaries are not pronounced, but some pores appear there. Despite spraying porous feedstock materials, extensive microporosity regions were not found, which in contrast with the results of Kear et al. (Ref 13). This microporosity was supposed to be caused by the heterogeneous melting of the porous feedstock particles. The pore size of the samples is different, being bigger for the conventional coating due to the bigger WC particle size.

The Vickers microhardness values of the samples are 1236 ± 238 and 1568 ± 93 HVN for the C1 and N1 coatings, respectively. As expected, the values for the nanostructured material are higher than those for the conventional material, and the dispersion of values is much lower for N1. The dissolution of WC into the Co matrix increases the matrix hardness by the solid solution of W and C into the Co. The resulting formation of the hard W_2C phase also increases the hardness of the coatings. However, other factors such as intersplat bonding, microporosity, and WC-matrix bonding should be taken into account. The resulting microhardness values will be a balance of all these contributions and can change along the coating. As the nanostructured coating has higher microhardness values, the solid solution strengthening by W and C and the finer WC distribution are the factors governing the microhardness of the coatings.

Figure 4 shows a TEM image of the N1 sample, in which two sizes of carbide WC crystals can be clearly seen. There are carbide WC crystals comprising sizes from 200 to 500 nm surrounded by smaller carbides of 10 to 50 nm. This particle size distribution was also seen in the starting powder. There are some rounded grains (in the center of Fig. 4) that must have been created after the deposition, as the starting powder was composed by faceted WC grains. They are expected to be W_2C grains because that morphology has been found by some researchers (Ref 21).

Figure 5 includes the diffraction pattern taken from the small WC grains in the N1 sample dark field image, showing the typical ring morphology of nanostructured materials (Ref 22).

3.2 Wear Tests

3.2.1 Sliding Test. The sliding test was performed, and the averages of the friction coefficients obtained from three tested samples of each coating were 0.206 ± 0.03 for the N1 coating and 0.294 ± 0.04 for the C1 coating. The plot for the sample that gave the intermediate value is shown in Fig. 6, where it can be seen that the C1 coating has a friction coefficient higher than that of N1. This trend has been reported before by Zhu et al. (Ref 25), who related the lower friction coefficient of nanostructured coatings.

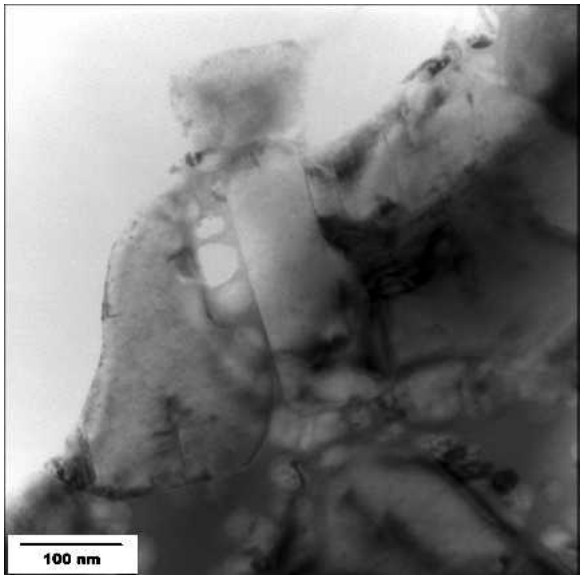

Fig. 4 TEM image of different sizes of WC grains in the nanostructured coating

The volume of material lost during the test was not possible to detect by means of white light interferometry because the wear path depth was below the resolution possible for this technique. In future work, the load and/or distance of the sliding test will be increased to enlarge the wear path. However, the width of the wear tracks studied using an SEM showed that the conventional coating had an average width of 450 μm, which was about two times that of the nanostructured coating (~250 μm). Considering the work of several authors, there seems to be a trend for increasing sliding wear resistance as microhardness increases. However, other factors such as W_2C content, WC grain size, and Co content can modify the sliding wear resistance for a given microhardness value (Ref 10, 26). Thus, the lower friction coefficient and the thinner wear path of the N1 coating lead to the conclusion that N1 has higher sliding wear resistance. Despite having more W_2C phase, the higher microhardness of the N1 coating seems to be the factor controlling wear resistance.

The study of the wear tracks after the BOD test corroborated some previous data about the wear mechanism. Oxides formed as the counterpart material (sintered WC-Co ball) slid over the sample (Ref 27, 28). The oxidation appeared along the wear path (dark areas), as can be seen in the secondary electrons (SE)-SEM images of the wear track (Fig. 7). The oxides accumulate in the fractured zones (removed splats by weak intersplat bonding) and are indicated by white arrows in Fig. 7.

Qiao et al. (Ref 1) proposed three wear mechanisms. Two of them have been seen in the studied samples: "wear of single WC grains," in which there is a preferential elimination of the Co matrix in some zones (A in Fig. 8a) followed by a decrease in the adhesion of WC grains due to the loss of matrix until WC grains are finally pulled out; and "lifting of entire splats", in which large areas of material are pulled out due to weak intersplat boundaries (B in Fig. 8a). The SEM images of the cross sections of both samples showed that the nanostructured coating had more lifted splat zones than the conventional coating due to the higher decarburization level reached. Then, these depleted zones are covered with a brittle oxide layer that breaks due to the applied load (Fig. 8a, b). At the same time, some WC grains break due to the counterpart load. This effect is especially visible in the conventional coatings, where small crushed WC grains remain spread over the whole path (C in Fig. 8a).

3.2.2 Abrasive Wear Test. Previous studies on bulk materials (Ref 29) have reported that sintered nanostructured WC-Co materials have higher abrasive resistance than their conventional counterparts. However, this improved abrasive resistance is not found in coatings deposited by HVOF spraying of nanostructured or conventional powders (Ref 2, 30, 31). Comparing nanostructured with conventional coatings, the former has lower wear resistance mainly due to the higher degree of decarburization, which leads to some detrimental processes. When dissolution takes place, flaws such as microporosity, creation of brittle W_2C phase, increasing of the Co-rich matrix percentage, and weak intersplat bonding are enhanced.

The measurements performed in this study showed that both materials have the same abrasive wear resistance after 30 min of testing, as can be seen in Fig. 9. The finer and more homogeneous distribution of WC particles and the reduction of the binder free path for abrading media when using nanostructured feedstock materials are the key factors for balancing the negative effects of the higher content of the brittle W_2C phase. Microhardness is another factor that some authors may take into account, although the relationship between hardness and abrasive wear resistance is not strong. However, as a result of the values obtained in this work, it seems that the higher microhardness (30% higher) obtained with nanostructured coatings should have a strong influence in the wear mechanism.

3.3 Electrochemical Tests

In Fig. 10, the E_{OC} plots for the studied samples and the steel substrate are shown. There is an initial potential decay for all samples due to the dissolution of oxides in the coating surface and also due to the penetration of the electrolyte. The potential stabilizes after 4 h of immersion for all of them. The E_{OC} value after 18 h is −0.39, −0.53, and −0.72 V, respectively, for N1, C1, and steel.

The nanostructured coating provides a corrosion protection to the substrate higher than the conventional one. The C1 sample shows an E_{OC} value that is closer to that of the steel. This suggests that the electrolyte has probably reached the substrate-coating interface after 18 h of immersion. The cross-sectional SEM images of both samples after E_{OC} tests showed that the C1 substrate-coating interface (Fig. 11a) was attacked. An EDS analysis confirmed the presence of ferrous oxides not only in the interface, but also in the coating surface. However, the N1 sample (Fig. 11b) withstood the electrolyte attack. There is no oxide formation either in the interface or in the coating surface. When the electrolyte reaches the interface, a coating detachment can occur after some testing for some hours (Ref 32, 33).

All Tafel polarization curves recorded after E_{OC} tests and impedance measurements are shown in Fig. 12. There is a current intensity decrease for the coatings in comparison with the steel substrate, showing the higher resistance of the coatings. Again, the N1 sample showed better corrosion protection for the substrate in this environment.

Electrochemical impedance spectroscopy measurements

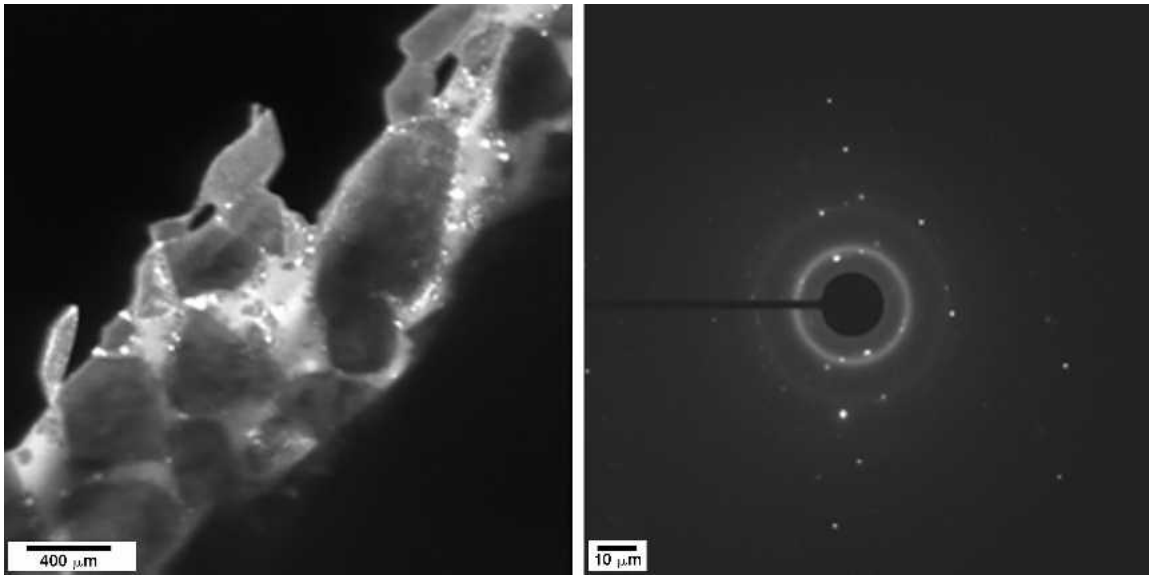

Fig. 5 Dark field TEM image of WC grains and the diffraction pattern of bright nanosized WC grains

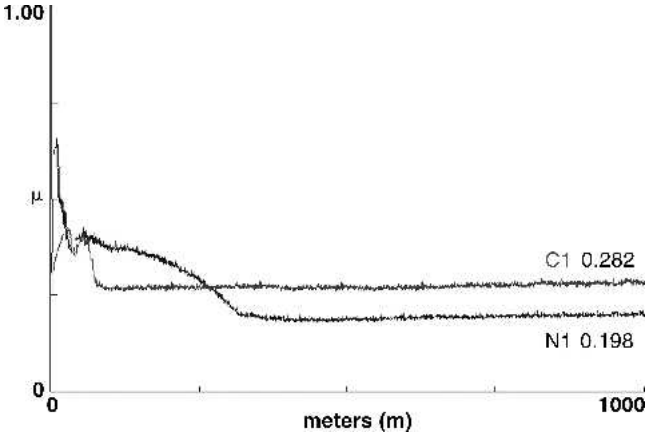

Fig. 6 Evolution of friction coefficient with covered distance for C1 and N1 samples

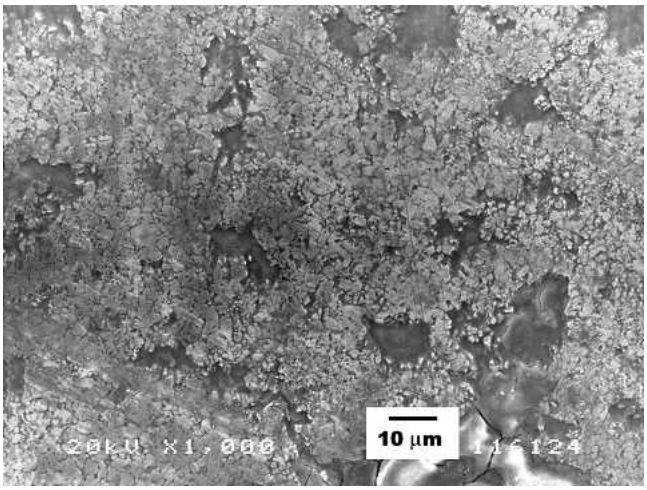

Fig. 7 SEM overview of the wear track for the conventional coating

were performed after stabilizing the E_{OC} and applying 5 mV (rms) on the E_{OC} value. The impedance data for the three evaluated systems are shown in Fig. 13. The results are shown as the Nyquist plot. The Nyquist plot allows the comparison of the capacitive semicircle of the samples. The bigger the capacitive semicircle, the higher the corrosion resistance. The N1 sample showed the highest capacitive semicircle, which means that it has higher corrosion resistance than the C1 coating.

The surface area of nanosized WC grain materials is higher than that of conventional materials, and the expected corrosion resistance for nanostructured coatings would be higher than that of conventional coatings, although several authors studying the WC-Co system have detected a preferential degradation of the Co matrix surrounding the WC grains (Ref 32). The N1 coating has provided better protection of the substrate from corrosion due to its nobler behavior and enhanced sealing properties, which attributed to its lower porosity. All of these results indicated that sealing properties have a strong role in corrosion resistance.

A salt fog spray test was also carried out to quantify the corrosion protection provided by N1 and C1 coatings. The C1 sample remained unaltered for 130 h, whereas the N1 sample withstood 600 h of testing. These results corroborate those qualitative results obtained from electrochemical tests. There is an increase of 350% in corrosion resistance for the N1 sample compared with the C1 sample.

4. Conclusions

- From the microstructural and XRD studies, it can be concluded that nanostructured coatings suffer more degradation in terms of decarburization and precipitation of W_2C.

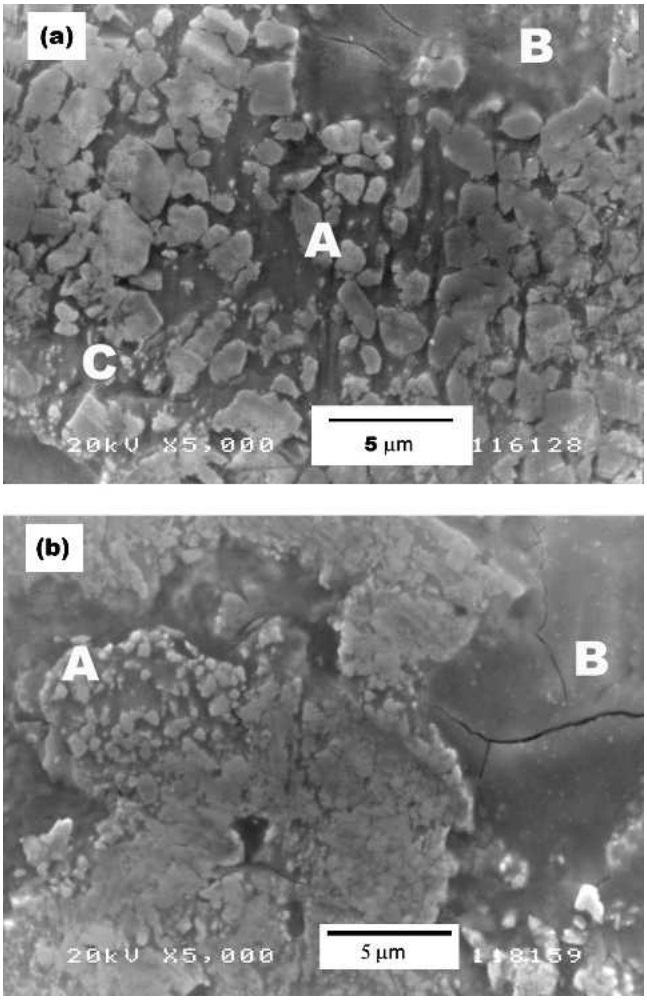

Fig. 8 SEM images of wear tracks after the BOD test for (a) the conventional coating and (b) the nanostructured coating

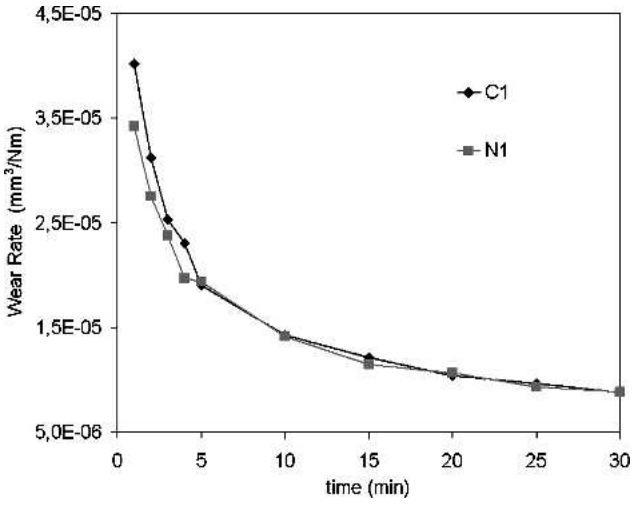

Fig. 9 Wear rate versus test time for conventional (C1) and nanostructured (N1) coatings

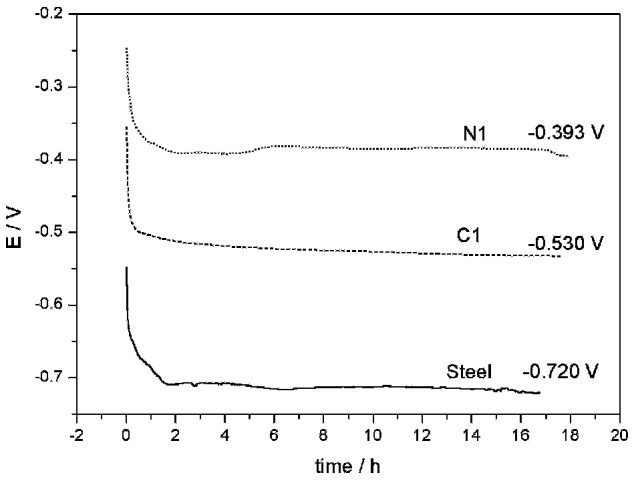

Fig. 10 E_{OC} plots of the samples and steel substrate after 18 h of immersion

The main reason for that is their larger surface-to-volume ratio. Because the spraying conditions were the standard conditions for the conventional powder, which were not optimized for the nanostructured powder, and also because both feedstock materials had the same porous morphology, the interaction of the particles with the flame only depends on the particle size because the nanostructured powder is finer and its degradation is higher. This effect has to be added to the surface-to-volume ratio effect.

- The Chung method has proved to be an effective tool for the quantification of the degree of decarburization endured by the particles. It showed that the W_2C-to-WC ratio increases as the decomposition increases, which is in agreement with that reported in the literature. The dissolution of WC grains in the Co matrix leads to an enrichment in W and C content. After the solidification of the splat, an amorphous W-C-Co matrix is created, which can be identified by XRD analysis by a hump in the region of 2θ 35° to 48°.
- The TEM studies showed that the nanostructured coating has two kinds of WC grains, called nanostructured WC grains, of about 10 to 50 nm and near-nanostructured WC grains of 200 to 500 nm. This was also observed in the initial powders by SEM. Some W_2C grains can be seen in the boundaries of the WC grains with the typical globular structure of the precipitated W_2C phase.
- The key factors in the microhardness of the nanostructured coating were the finer distribution of carbides in the matrix and the hardening effect of W and C dissolution in the Co matrix. As a result, the nanostructured coating showed higher hardness (around 30%) and lower dispersion of the obtained results compared with the conventional coating.
- The friction coefficient of the N1 coating was 30% lower than that of the C1, and the wear path was also thinner. The nanostructured coating showed better sliding wear behavior than the conventional coating. The higher microhardness of the nanostructured coating seems to be the factor controlling the sliding wear resistance.
- The higher level of the W_2C phase in the nanostructured

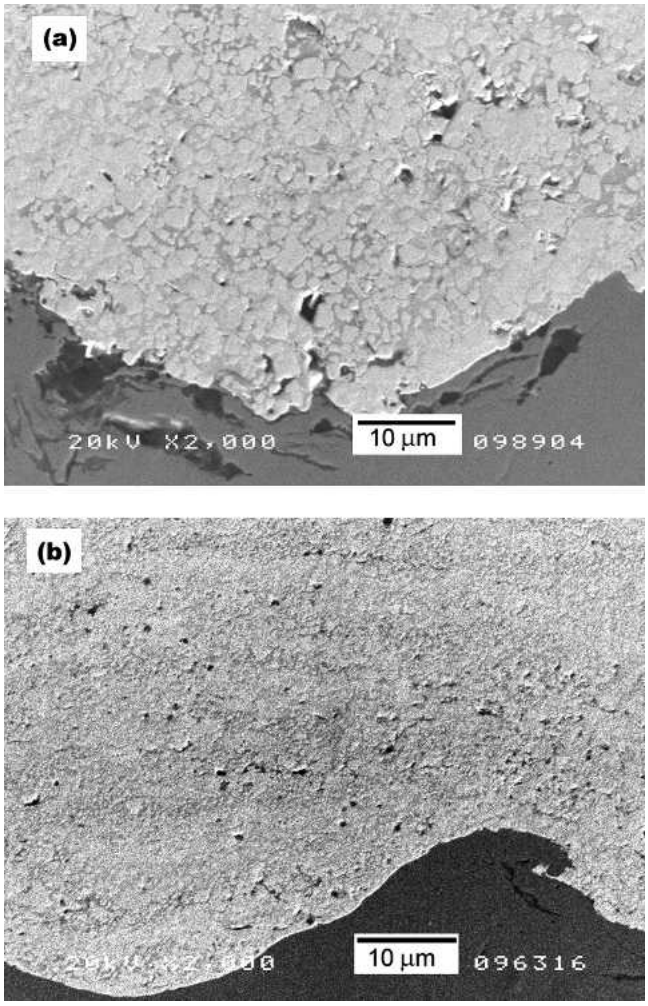

Fig. 11 Cross-sectional SEM images for (a) conventional and (b) nanostructured coatings after electrochemical tests

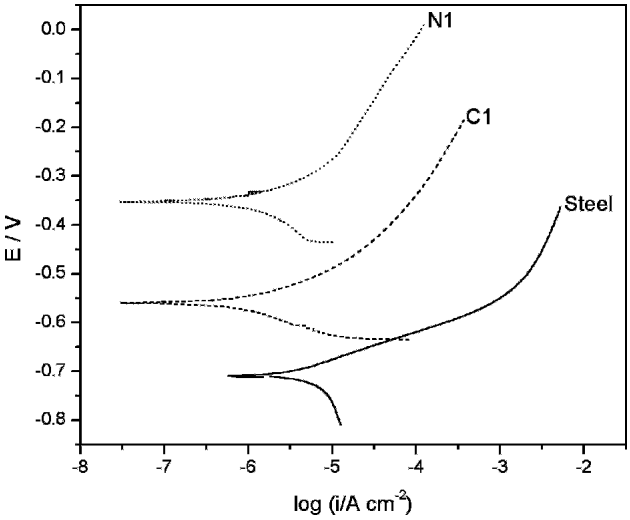

Fig. 12 Tafel plots for samples N1, C1, and the steel substrate

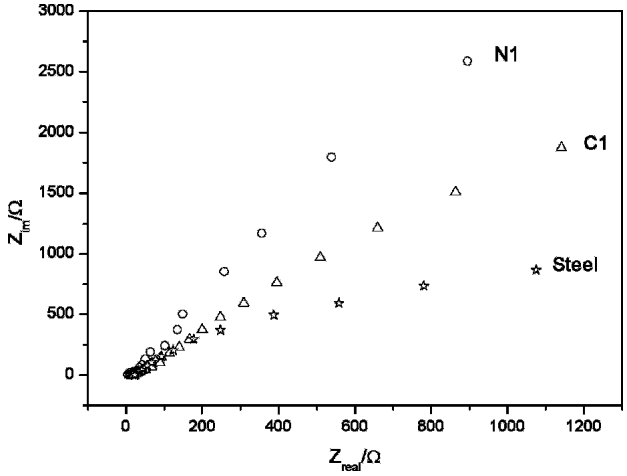

Fig. 13 Nyquist plot for samples N1, C1, and the steel substrate

coating has weakened intersplat bonding, and thus more splat debonding has occurred in the N1 samples. Brittle oxide layers are created in detached areas. The typical mechanism of the preferential wear of Co matrix followed by WC grain detachment takes place in both coatings, although an additional wear mechanism consisting on crushing WC grains can be observed in the conventional coating.

- The nanostructured and conventional coatings have shown the same abrasive wear resistance. The finer and more homogeneous distribution of WC particles and the reduction of the binder free path for abrading media when using nanostructured feedstock materials are the key factors for balancing the negative effects of the higher content in the brittle W_2C phase. In addition, it seems that the higher microhardness obtained with the nanostructured coating should have a strong influence on the wear mechanism as well.
- Electrochemical tests and salt fog spray test corroborate that the nanostructured coating shows higher corrosion resistance than the conventional coating. The N1 coating showed a 3.5 times higher corrosion protection for the substrate compared with that of the C1 coating in the salt fog test. This superior performance is credited to its overall sealing properties.
- Even though the properties of the nanostructured coating sprayed under nonoptimized spraying conditions are better than those for the conventional coating, an optimization of the process might be required.

Acknowledgments

The authors S. Dosta and J. Nin wish to thank the University of Barcelona for the financial support for this research. This research was also supported by the Ministerio de Educación y Ciencia under project MAT 2003-05004-C02-02 and by the Generalitat de Catalunya under project 2001 SGR 00145.

References

1. Y. Qiao, T.E. Fischer, and A. Dent, The Effects of Fuel Chemistry and Feedstock Powder Structure on the Mechanical and Tribological Prop-

erties of HVOF Thermal-Sprayed WC-Co Coatings with Very Fine Structures, *Surf. Coat. Technol.,* Vol 172, 2003, p 24-41
2. A. Dent, S. DePalo, and S. Sampath, Examination of the Wear Properties of HVOF Sprayed Nanostructured and Conventional WC-Co Cermets with Different Binder Phase Contents, *J. Thermal Spray Technol.,* Vol 11 (No. 4), 2002, p 551-558
3. B.R. Marple, J. Voyer, J.F. Bisson, and C. Moreau, Thermal Spraying of Nanostructured Cermet Coatings, *J. Mater. Proc. Technol.,* Vol 117, 2001, p 418-423
4. H. Chen, X Zhou, and C. Ding, Investigation of the Thermomechanical Properties of a Plasma-Sprayed Nanostructured Zirconia Coating, *J. Eur. Ceram. Soc.,* Vol 23, 2003, p 1449-1455
5. R.S. Lima, U. Senturk, C.C. Berndt, and C.R.C Lima, Spraying Characteristics of Nanostructured Zirconia Particles, Tagungsband Conference Proceedings, E. Lugscheider and P.A. Kammer, Ed., March 17-19, 1999 (Dusseldorf, Germany), DVS Deutscher Verband für Schweissen, 1999, p 190-195
6. M. Gell, E.H. Jordan, Y.H. Sohn, D. Goberman, L. Shaw, and T.D. Xiao, Development and Implementation of Plasma Sprayed Nanostructured Ceramic Coatings, *Surf. Coat. Technol.,* Vol 146-147, 2001, p 48-54
7. B.H. Kear, Z. Kalman, R.K. Sadagi, G. Skandan, J. Colazzi, and W.E. Mayo, Plasma-Sprayed Nanostructured Al_2O_3/TiO_2 Powders and Coatings, *J. Thermal Spray Technol.,* Vol 9 (No. 4), 2000, p 483-487
8. R. Soltani, T.W. Colye, and J. Mostaghimi, Wear Resistance of Nanostructured Thermal Barrier Coatings, *Thermal Spray 2003: Advancing the Science and Applying the Technology,* B.R. Marple and C. Moreau, Ed., May 5-8, 2003, ASM International, 2003, Vol 2, p 1535-1540
9. K. Jia and T.E. Fischer, Abrasion Resistance of Nanostructured and Conventional Cemented Carbides, *Wear,* Vol 200, 1996, p 206-214
10. K. Jia and T.E. Fischer, Sliding Wear of Conventional and Nanostructured Cemented Carbides, *Wear,* Vol 203-204, 1997, p 310-318
11. B.R. Marple and R.S. Lima, Process Temperature-Hardness-Wear Relationships for HVOF-Sprayed Nanostructured and Conventional Cermet Coatings. *Thermal Spray 2003: Advancing the Science and Applying the Technology,* C. Moreau and B. Marple, Ed., May 5-8, 2003 (Orlando, FL), ASM International, 2003, p 273-282
12. J. Delgado, "Fenomenología y Caracterización de la Resistencia a la Corrosión Electroquímica en Diversos Medios Agresivos de Recubrimientos Obtenidos por Proyección Tèrmica," Ph.D. dissertation, University of Barcelona, Barcelona, 08028, Spain, 2001 (in Spanish)
13. B.H. Kear, G. Skandan, and R.K. Sadangi, Factors Controlling Decarburization in HVOF Sprayed Nano-WC/Co Hardcoatings, *Scripta Mater.,* Vol 44, 2001, p 1703-1707
14. F.H. Chung, Quantitative Interpretation of X-Ray Diffraction Patterns of Mixtures: I. Matrix-Flushing Method for Quantitative Multicomponent Analysis, *J. Appl. Cryst.*, Vol 7*,* 1974, p 519-525
15. F.H. Chung, Quantitative Interpretation of X-Ray Diffraction Patterns of Mixtures. II. Adiabatic Principle of X-Ray Diffraction Analysis of Mixtures, *J. Appl. Cryst.*, Vol 7*,* 1974, p 526-531
16. "Standard Test Method for Wear Testing with a Pin-on-Disc Apparatus," G99-90, *Annual Book of ASTM Standards*, ASTM, 1990
17. "Standard Test Method for Wear Measuring Abrasion Using the Dry Sand/Rubber Wheel Apparatus," G65-91 D, *Annual Book of ASTM Standards*, ASTM, 1991, p 239-251
18. F. Mansfeld, S. Lin, Y.C. Chen, and H. Shih, Minimization of High-Frequency Phase Shifts in Impedance Measurements, *J. Electrochem. Soc.*, Vol 135, 1998, p 906-907
19. A. Boukamp, *Equivalent Circuits, Users Manual*, 2nd ed., Universiteit Twente, Enschede, The Netherlands, 1989
20. "Standard Test Method of Salt Spray (Fog) Testing," B117-90, Annual Book of ASTM Standards, ASTM, 1990
21. J.M. Guilemany, J.M. de Paco, J. Nutting, and J.R. Miguel, Characterization of the W_2C Phase Formed During the HVOF Spraying of a WC-12Co Powder, *Metall. Mater. Trans. A,* Vol 30, 1999, p 1913-1921
22. C. Verdon, A. Karimi, and J.-L. Martín, A Study of High Velocity Oxy-Fuel Thermally Sprayed Tungsten Carbide Based Coatings: Part 1. Microstructures, *Mater. Sci. Eng., A*, Vol 246, 1998, p 11-24
23. J. He and J.M. Schoenung, Nanostructured Coatings, Review, *Mater. Sci. Eng.. A*, Vol 336, 2002, p 274-319
24. V.V. Sobolev, J.M. Guilemany, and J. Nutting, *High Velocity Oxy-Fuel Spraying,* W.S. Maney and Son Ltd., Leeds, UK, 2004
25. Y. Zhu, K. Yukimura, C. Ding, and P. Zhang, Tribological Properties of Nanostructured and Conventional WC-Co Coatings Deposited by Plasma Spraying, *Thin Solid Films*, Vol 388, 2001, p 277-282
26. Y. Qiao, Y. Liu, and T.E. Fischer, Sliding and Abrasive Wear Resistance of Thermal-Sprayed WC-Co Coatings, *J. Thermal Spray Technol.,* Vol 10 (No. 1), 2001, p 118-125
27. J.M. Miguel, "Caracterización Estructural y de Propiedades Tribológicas y Mecánicas de Recubrimientos de Interés Tecnológico Obtenidos por Proyección Térmica," Ph.D. dissertation, University of Barcelona, Barcelona, Spain, 2002 (in Spanish)
28. V. Fervel, B. Normand, H. Liao, C. Coddet, E. Bêche, and R. Berjoan, Friction and Wear Mechanisms of Thermally Sprayed Ceramic and Cermet Coatings, *Surf. Coat. Technol.,* Vol 111 (No. 2-3), 1999, p 255-262
29. K. Jia and T.E. Fischer, Abrasion Resistance of Nanostructured and Conventional Cemented Carbides, *Wear,* Vol 200, 1996, p 206-214
30. D.A. Stewart, P.H. Shipway, and D.G. McCartney, Abrasive Wear Behavior of Conventional and Nanocomposite HVOF-Sprayed WC-Co Coating, *Wear,* Vol 225-229, 1999, p 789-798
31. G. Skandan, M. Jain, T.E. Fischer, B.H. Kear, W.R. Rigney, R. Shropshire, and S. Brunhouse, On the Influence of Powder Feed Structure on Wear Properties of HVOF Sprayed WC-Co Hardcoatings, *Thermal Spray: Surface Engineering via Applied Research,* C.C. Berndt, Ed., May 8-11, 2000 (Montréal, Québec, Canada), ASM International, 2000, p 971-976
32. J.M. Guilemany, P. Cabot, and J. Fernández, Electrochemical Corrosion of Cermet Coatings in Artificial Marine Water, *Mater. Sci. Forum,* Vol 289/292 (No. 2), 1998, p 667-678
33. P.H. Suegama, C.S. Fugivara, A.V.Benedetti, J.Fernández, J. Delgado, and J.M. Guilemany, Electrochemical Behavior of Thermally Sprayed Cr_3C_2-NiCr Coatings in 0.5 M H_2SO_4 Media, *J. Appl. Electrochem.,* Vol 32, 2002, p 1287-1295